Time-Domain Response Analysis of a Flexible Structure Embedded in Porous Soil

by

Xiu LUO[1], Kazuo KONAGAI[1], Assadollah NOORZAD[2]

ABSTRACT

Many problems in earthquake engineering relate to the dynamic behavior of saturated porous soil. Saturated porous soil is the material composed of solid and fluid phases, which manifests obvious deforming and diffusing characteristics under dynamic loading. Thus, it is necessary to take into account these characteristics in dealing with a porous soil-structure interaction problem. In the present approach, the porous soil surrounding a foundation is sliced into a number of elements taking into account various wave radiation patterns. The soil impedance functions for various vibration modes are then well approximated by the syntheses of springs and dashpots. The parameters of the models are thus dependent on the equivalent Poisson's ratio, but not on the excitement frequency at all. The equivalent Poisson's ratio is the function of the degree of saturation, permeability coefficient and porosity of the porous soil. From the numerical examples, it is found possible for the equivalent Poisson's ratio to be quite different from the one obtained from the in-situ PS logging, depending on the permeability and porosity of the soil.

INTRODUCTION

Modeling the unbounded soil is a key task in dealing with a soil-structure interaction problem. It is not seldom that the soil is idealized as a continuous mono-phase material and the stiffness of the soil supporting a structure is expressed as a complex function in the frequency-domain so that the effect of wave dissipation into the unbounded soil can be taken into account. In reality, however, soil consists of porous granular fabric partly-permeated or perfectly-saturated by water. In many cases, the effect of the interaction between the solid and the fluid phase may not be negligible. Furthermore, when the nonlinear feature of the porous soil surrounding an embedded structure is discussed, the time-domain analysis seems to be preferable to the frequency-domain one. Therefore, it is necessary to develop a time-domain approach to solve the porous soil-structure interaction problems. This paper extends the time-domain study of soil-structure interaction by Nogami and Konagai (1986, 1987, 1988) so that the solid-fluid interaction within the porous soil can be rationally taken into account. Being based on Biot's theory and the plane strain wave propagation model, the impedance functions of a rigid disk embedded in an infinite porous plane are derived. Since the analytical solutions are too complicated to be directly transformed into time-domain expressions, the impedance functions are expressed in terms of frequency-independent parameters. In the present approach, the model

[1]Xiu LUO, [1]Kazuo KONAGAI, *Institute of Industrial Science, University of Tokyo*
[2]Assadollah NOORZAD, *Dept. of Civil Engineering, Tehran University*

parameters are expressed as functions of equivalent Poisson's ratio, that reflects the effect of the bulk moduli of fluid and solid phases, permeability and porosity of soil. In numerical examples, the present impedance functions are attached to an embedded upright Timoshenko-type beam, which represents a flexural embedded body like a slender caisson or a pile group, and the time-domain response analysis of the structure is conducted by taking porous soil profiles from Kobe as examples.

POROUS SOIL-STRUCTURE INTERACTION FORCE IN TIME-DOMAIN

In cylindrical coordinate, the governing equations of a porous medium can be expressed into three separate sets of partial differential equations, in terms of displacement potentials,

$$\begin{bmatrix} \lambda^* + 2\mu^* + Q & Q \\ Q & Q \end{bmatrix} \nabla^2 \begin{Bmatrix} \phi \\ \psi \end{Bmatrix} = \begin{bmatrix} \rho & \rho_f \\ \rho_f & \alpha\rho_f / n \end{bmatrix} \frac{\partial^2}{\partial^2 t} \begin{Bmatrix} \phi \\ \psi \end{Bmatrix} + \begin{bmatrix} 0 & 0 \\ 0 & b \end{bmatrix} \frac{\partial}{\partial t} \begin{Bmatrix} \phi \\ \psi \end{Bmatrix}$$
$$\begin{bmatrix} \mu^* & 0 \\ 0 & 0 \end{bmatrix} \nabla^2 \begin{Bmatrix} H_j \\ G_j \end{Bmatrix} = \begin{bmatrix} \rho & \rho_f \\ \rho_f & \alpha\rho_f / n \end{bmatrix} \frac{\partial^2}{\partial^2 t} \begin{Bmatrix} H_j \\ G_j \end{Bmatrix} + \begin{bmatrix} 0 & 0 \\ 0 & b \end{bmatrix} \frac{\partial}{\partial t} \begin{Bmatrix} H_j \\ G_j \end{Bmatrix} \quad (j = 1,2) \tag{1}$$

where, $\lambda^*=\lambda(1+i(da))$, $\mu^*=\mu(1+i(da))$, λ and μ = Lame's constants, da = hysteresis damping ratio of solid phase, $\rho=(1-n)\rho_s+n\rho_f$ = density of soil, ρ_s = density of solid, ρ_f = density of fluid, n= porosity, p = atmospheric pressure, $Q=1/(n(1/k_f+(1-s)/p))$= bulk modulus of fluid-gas mixture, s = degree of saturation, k_f = bulk modules of fluid, $\alpha=2/n-1$= toruosity for spherical shapes, showing mass coupling effect of phases, $b=gn\rho_f/k$= diffusive coefficient, g=gravitational acceleration, k = permeability coefficient of soil, ϕ, H_j = the potentials of the displacement of solid phase, ψ, G_j = the potentials of the relative displacement between the solid and fluid phases and ∇ = gradient, respectively. The variations of ϕ, ψ are associated with volumetric wave propagation, whereas H_j, G_j show distortional wave propagation.

Finding the eigen values and eigen vectors of Eq.(1) allows Eq.(1) to be decoupled with respect to both ϕ and ψ. Substituting the boundary conditions in the equations of ϕ and ψ, and after mathematical manipulation, the impedance functions of a rigid disk embedded in a plane strain porous medium with an infinite extent are analytically available for various vibration modes(Noorzad and Konagai, 1993). The impedance function for swaying motion is expressed in the following form as:

$$K_h = \pi\mu(a_3^*)^2 \frac{R_2}{R_3} \tag{2}$$

where, $a_j^* = i\beta_j r_0$, $(j=1,2,3)$, $\beta_j = \frac{\omega}{v_p^*}\lambda_j$ $(j=1,2)$, $\beta_3 = \frac{\omega}{v_s^*}\lambda_3$, K_m= the second modified complex Bessel function of order m, λ_j= the eigen values of Eq.(1).

$$R_2 = K_1(a_3^*)(4K_1(a_1^*) + a_1^* K_0(a_1^*) + 4R_1 K_1(a_2^*) + R_1 a_2^* K_0(a_2^*)) + a_3^* K_0(a_3^*)(K_1(a_1^*) + R_1 K_1(a_2^*))$$

$$R_3 = a_3^* K_0(a_3^*)(K_1(a_1^*) + R_1 K_1(a_2^*) + a_1^* K_0(a_1^*) + R_1 a_2^* K_0(a_2^*)) + K_1(a_3^*)(a_1^* K_0(a_1^*) + R_1 a_2^* K_0(a_2^*))$$

$$R_1 = \begin{cases} \dfrac{(1+t_{21})\beta_1^2 K_1(i\beta_1 r)}{(1+t_{22})\beta_2^2 K_1(i\beta_2 r)} A_2 & \text{For the drained condition} \\ \dfrac{t_{21}\beta_1^2 K_1(i\beta_1 r)}{t_{22}\beta_2^2 K_1(i\beta_2 r)} A_2 & \text{For the undrained condition} \end{cases}$$

The variation of stiffness ratio (k_h/μ) with respect to both the normalized frequency a_0 and the permeability coefficient k is shown in Fig. 1. The real part of the stiffness is getting more and more downward to the right as the permeability coefficient decreases, whereas the imaginary part is affected little by the change in the permeability.

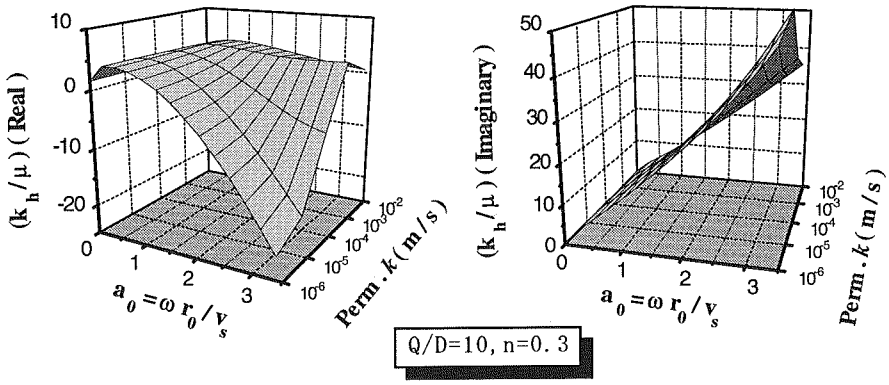

Fig. 1 *Variation of the stiffness of porous medium for swaying motion with dimensionless frequency and permeability, the bulk modulus of solid phase* $D=2.0\times10^4 tf/m^2$ *and fluid phase* $Q=2.0\times10^5 tf/m^2$, *the mass density of solid phase* $\rho_s=2.6t/m^3$ *and the coefficient of hysteresis damping* $da=0.0$

The impedance function for the rocking motion of a rigid disk is given as:

$$K_{rp} = \pi\mu r^2 (1+da)(1+a_3^* \frac{K_0(a_3^*)}{K_1(a_3^*)}) \qquad (3)$$

Fig. 2 shows the variation of the rocking stiffness with respect to the normalized frequency and the permeability coefficient. Differing from the case of horizontal motion, both the real and imaginary parts vary slightly with the permeability coefficient. Fig. 1, when compared with Fig. 2, implies that the effect of permeability on the impedance variation appears when the volumetric deformation is accompanied by the wave radiation, because the interaction between the solid and fluid phases affects the pore pressure generation. For this reason, the effect of pore pressure generation can be discussed in the time-domain only when the volumetric wave exists.

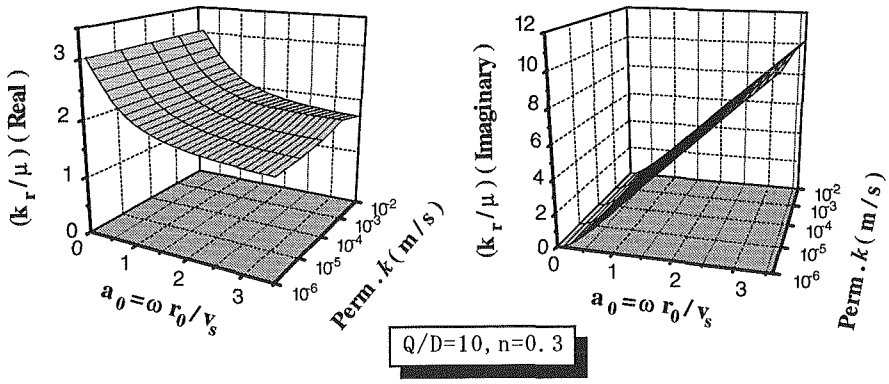

Fig. 2 *Variation of the stiffness of porous medium for rocking motion with dimensionless frequency and permeability*

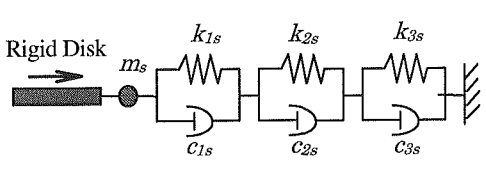

$$k_h(\omega)=\mu\xi_k(\upsilon_E)\left(\sum_j \frac{1}{\tilde{k}_j+i\tilde{c}_j a_0}\right)^{-1}-\mu\xi_m(\upsilon_E)a_0^2$$

Fig. 3 *Soil model for swaying motion*

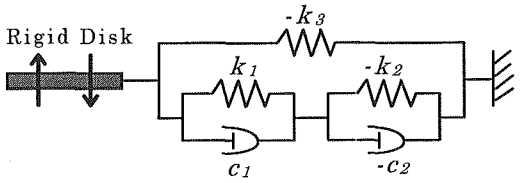

$$k(\omega)=\frac{k_1k_2-k_3(k_2-k_1)+\{k_1c_2+k_2c_1-k_3(c_2-c_1)\}a_0-c_1c_2a_0^2}{(k_2-k_1)+(c_2-c_1)a_0}$$

Fig. 4 *Soil model for rocking motion*

Since the analytical form of the above-mentioned impedance functions are still hard to be directly transformed into the time-domain expressions, the method for modeling impedance functions in terms of frequency-independent parameters (Nogami and Konagai, 1988) is used in the present approach. According to the approach taken by Nogami and Konagai, the reaction to the dynamic lateral motion of an embedded massless disk is well approximated by a synthesis of a couple of Voigt models arranged in series with an added mass at the end (Fig. 3), and three voigt models allows the precise approximation to be obtained within the frequency range, $0.02<a_0<10$. Concerning the rocking motion of the embedded disk, Konagai (1995) also showed that the approximate impedance function of the disk in the frequency domain (Nogami and Sun) is well approximated by the synthesis of springs and dashpots illustrated in Fig. 4. The spring constants, damping constants of the dashpots and the added mass for the models are frequency-independent, and the functions of Poisson's ratio when the motion of disk generates volumetric waves. Therefore, it would be rational to think over the possibility of incorporating the effect of pore-pressure generation just by introducing the equivalent Poisson's ratio as the function of the bulk moduli of solid and fluid phases, permeability and porosity of soil.

Reviewing some soil profiles along the elevated section of the Hanshin expressway, Kobe, that suffered the devastating damage by the Jan. 17 earthquake of 1995, parameters for describing the three typical soils are set at the values listed in Table 1. The bulk modulus of water Q entrapping air bubbles is noticeably reduced, when compared with the state of perfect saturation, and the modulus depends strongly on the degree of saturation.

Table 1. *Approximate values for parameters of some typical soils in the area of Kobe*

Soil type	Porosity n	ρ_s (g/cm^3)	k (m/s)	$Q/(D=\lambda+2\mu)$ *(s=0.95)*	$Q/(D=\lambda+2\mu)$ *(s=1.0)*
Diluvial sand or gravel	0.15-0.45	2.6-2.7	10^{-2}-10^{-4}	0.0082	8.99
Alluvial sand	0.2-0.5	2.6-2.7	10^{-2}-10^{-6}	0.036	39.6
Silt or alluvial clay	0.3-0.55	2.5-3.1	10^{-8}-10^{-10}	5.66	6180

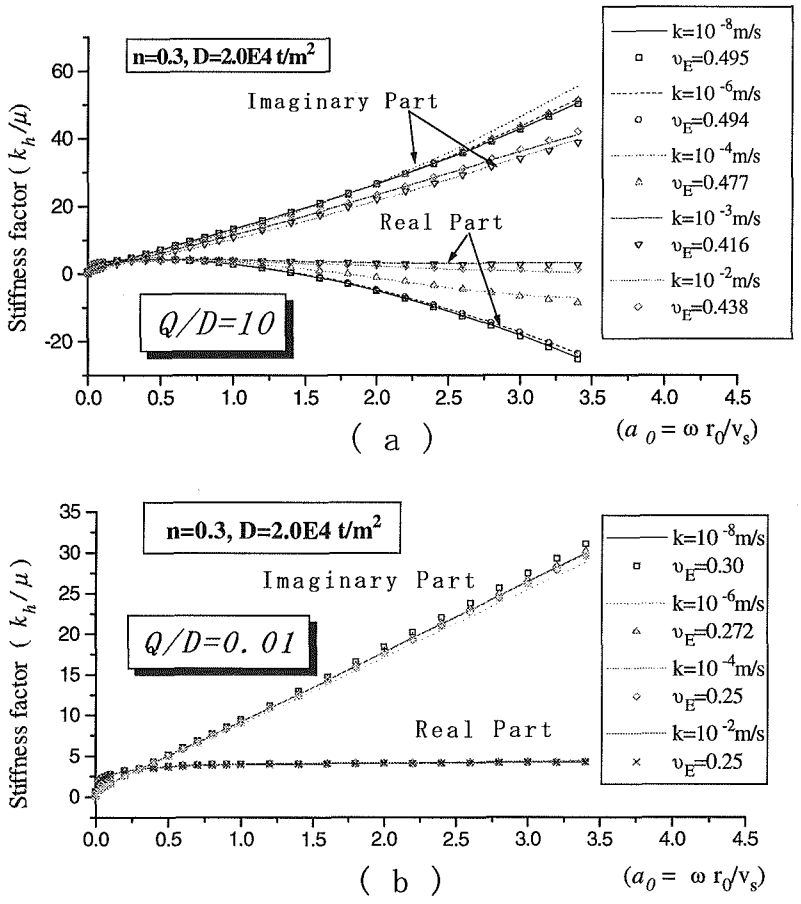

Fig. 5 *Comparison of the stiffness calculated by the model of porous medium and the model of continuous medium with equivalent Poisson's ratio*

Fig. 5-a and Fig. 5-b show the variations with frequency of both real and imaginary parts of the horizontal impedance functions for different values of permeability coefficients, with the other parameters being set at the prescribed values (n = 0.3, Q/D = 10, D = 2.0×10^4 t/m^2). The open marks are the approximate solutions by the present approach. The best fit to the rigorous solutions is obtained setting the equivalent Poisson's ratios at the values in the legend. The equivalent Poisson's ratio increases as the permeability decreases (Fig. 5-a). On the other hand, the change in the permeability affects little the equivalent Poisson's ratio when the bulk modulus of the fluid phase is low (Fig. 5-b).

Fig. 5-a offers an important revelation that it is quite possible that the equivalent Poisson's ratio for a completely saturated soil is much smaller than the one from the PS logging. It is not seldom that the PS logging provides the measured longitudinal wave velocity of about 1500m/s, which is equal to the velocity of the sound through water, thus yielding the Poisson's ratio of about 0.5. As is shown in the figure, the higher the normalized frequency is, the clearer the effect of Poisson's ratio on the impedance function is. Therefore the soil parameters must be carefully determined especially when a thick foundation with a large representative size is embedded in a water-saturated loose sandy soil deposit with comparatively high permeability.

TIME-DOMAIN APPROACH FOR EMBEDDED FLEXIBLE FOUNDATION

When an embedded body is a flexible structure like a slender caisson or a pile group, the beam of Timoshenko type would be preferable to the one of Beronoulli-Euller type for the model of the embedded body.

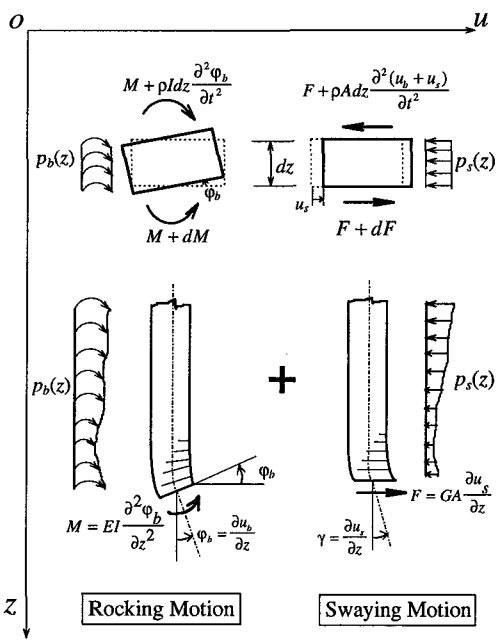

Fig. 6 *Discretization of a Timoshenko beam*

Governing equations of a Timoshenko beam supported by the soil springs of Winkler type (Fig. 6) are given as:

$$\rho A\frac{\partial^2(u_b+u_s)}{\partial t^2}=GA\frac{\partial^2 u_s}{\partial x^2}-p_s(z)$$

$$\rho I\frac{\partial^2\varphi_b}{\partial t^2}=EI\frac{\partial^2\varphi_b}{\partial x^2}+GA\frac{\partial u_s}{\partial x}-p_b(z) \qquad (4),(5)$$

where, u_b, u_s = the lateral deformations due to bending and shearing, respectively. $\varphi_b=\partial u_b/\partial z$, p_s and p_b are the lateral reaction force and moment of soil for swaying and rocking motion, respectively. The formulae shown in Fig. 3 and Fig. 4 are used to express the reaction forces p_s and p_b, respectively. According to the Winkler's hypothesis, p_s and p_b are determined only by the displacement at the

depth z. The loading time history is digitized at time increment Δt. In the step-by-step analysis, p_s and p_b at time t_i is expressed as:

$$p_{s,i} = k_s(u_{b,i} + u_{s,i} - u_{g,i}) + d_{s,i}$$
$$p_{b,i} = k_b\varphi_{b,i} + d_{\varphi,i} \qquad (6),(7)$$

where, $d_{s,i}$ and $d_{\varphi,i}$ are given as constants at t_i, which are determined using known displacements, velocities and accelerations at the previous time step t_{i-1}. By assuming that the increment of acceleration is proportional to $(t - t_{i-1})^{\alpha}$, the accelerations $\ddot{u}_{b,i}$, $\ddot{u}_{s,i}$ and $\ddot{\varphi}_{b,i}$ can be expressed as:

$$\ddot{u}_{b,i} = \xi_a u_{b.i} - \zeta^a_{b,i}$$
$$\ddot{u}_{s,i} = \xi_a u_{s.i} - \zeta^a_{s,i} \qquad (8),(9),(10)$$
$$\ddot{\varphi}_{b,i} = \xi_a \varphi_{b.i} - \zeta^a_{\varphi,i}$$

where, $\xi_a = \dfrac{(\alpha+1)(\alpha+2)}{\Delta t^2}$, $\zeta^a_{b,i}$, $\zeta^a_{s,i}$ and $\zeta^a_{\varphi,i}$ are the functions of displacements, velocities and accelerations at the previous time step, respectively (Nogami and Konagai, 1986). Substituting Eqs. (6), (7) and (8)-(10), into Eqs. (4), (5), the following equations are obtained:

$$\rho A\{\xi_a(u_{b,i} + u_{s,i}) - \zeta^a_{b,i} - \zeta^a_{s,i}\} = GA\frac{d^2u_{s,i}}{dx^2} - \{k_s(u_{b,i} + u_{s,i} - u_{g,i}) + d_{s,i}\}$$
$$\rho I(\xi_a\frac{du_{b,i}}{dx} - \zeta^a_{\varphi,i}) = EI\frac{d^3u_{b,i}}{dx^3} + GA\frac{du_{s,i}}{dx} - (k_b\frac{du_{b,i}}{dx} + d_{\varphi,i}) \qquad (11),(12)$$

Both the displacements $u_{s,i}$ and $u_{b,i}$ within a segment are assumed to be expressed in polynomial form as:

$$u_{s,i} = C_{s3,i}x^3 + C_{s2,i}x^2 + C_{s1,i}x + C_{s0,i}$$
$$u_{b,i} = C_{b4,i}x^4 + C_{b3,i}x^3 + C_{b2,i}x^2 + C_{b1,i}x + C_{b0,i} \qquad (13),(14)$$

There are 9 unknown constants ($C_{sj,i}$ and $C_{bj,i}$) in the above equations. In the transfer matrix approach, 5 physical quantities are transferred from one end of the segment to another. They are: *(1)* displacement due to swaying $u_{s,i}$, *(2)* displacement due to rocking $u_{b,i}$, *(3)* rotation angle $\varphi_{b,i}$, *(4)* shear force $GA(du_{s,i}/dz)$ and *(5)* moment $EI(d^2u_{b,i}/dx^2)$. These quantities are given at the both ends of the segment. Therefore, the total 10 quantities are expressed in terms of the 9 unknown constants by using Eqs. (13)(14). Moreover, the governing equations (11), (12) should be satisfied at the both ends of the segment, that is, another 4 equations are added. As the consequence, total 14 equations are available. Hence, any 9 equations out of these 14 are used to determine the 9 unknown constants and, the transfer matrix can be formulated by using another 5 equations left. After building up the transfer matrixes, there are 10 unknown quantities on the top and bottom ends of the beam. Therefore, 5 boundary conditions are seemingly needed to be given in the process of step-by-step computation. However, it is noted that either or both of $u_{b,i}(z)$ and $u_{s,i}(z)$ could be shifted to any extent as far as the displacement compatibility is satisfied at the boundaries. In other words for example, it would be possible to

replace $u_{b,i}(z)$ with $u_{b,i}(z)+B_i$ so that the bottom displacement $u_{b,i}(z_{bottom})+B_i$ is equal to any arbitrarily chosen constant C. Thus, only 4 boundary conditions are needed.

NUMERICAL EXAMPLES AND IMPLICATIONS

An embedded cylinder shown in Fig. 7 with an inverted pendulum on its top is considered. Two extreme cases of soil profiles are set up within the possible extents of parameters for the soils shown inFig. 7. Case 1 premises the presence of the comparatively impermeable sandy soil fill, probably with finer grains mixed in, over the subsurface alluvial clay, whereas a permeable soil fill overlies the subsurface material in case 2. The acceleration time history recorded at the Kobe Marine Meteorological Observatory, Jan. 17, 1995, is input, through a dashpot, to the stiffer soil layer beneath the depth of embedment (-29m). The dashpot represents the effect of energy dissipation by the waves going down into an infinite extent. The acceleration time history, in which the peak value of 818cm/s^2 has been reached, is noticeably strong enough for the nonlinear response analysis to be indispensable. In the first place, however, the time-domain soil-foundation interaction is discussed in terms of linear elasticity for the solid phase, even though the present approach has the capability of incorporating nonlinear behavior of porous medium. The subject of discussion is thus the effect of the permeability of soil on the dynamic response of the soil-structure system.

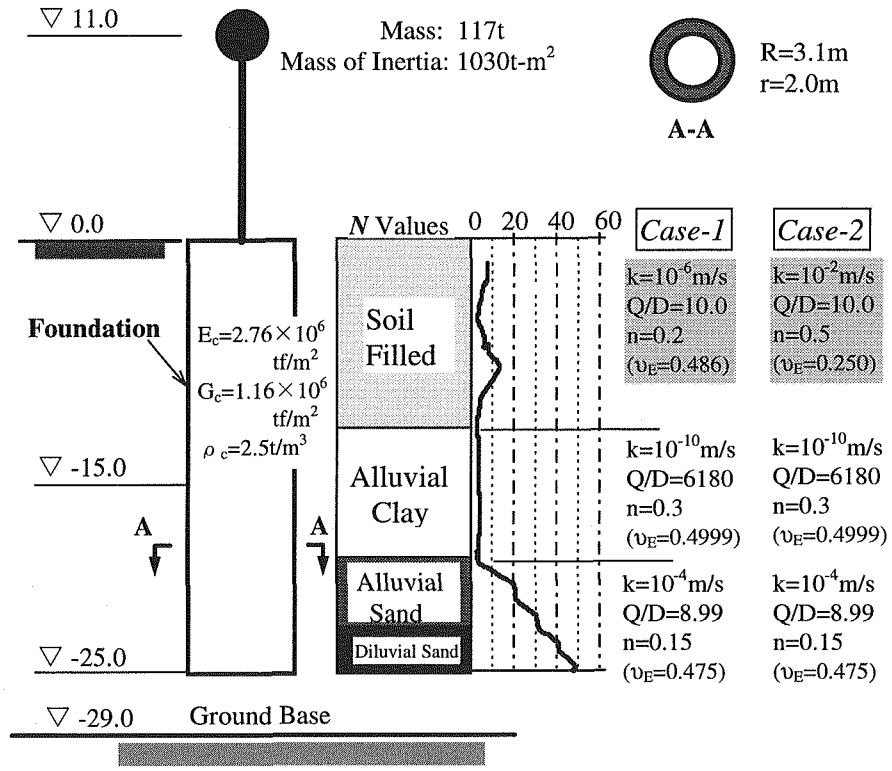

Fig. 7 *The sketch of the foundation with the soil profile*

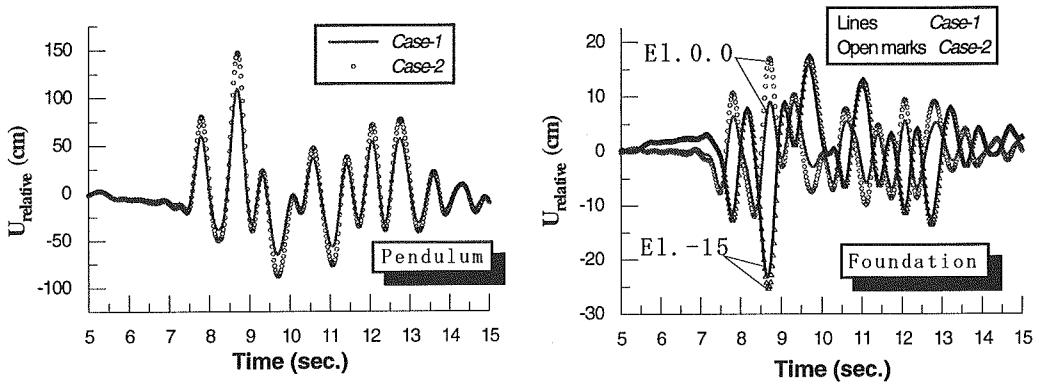

Fig. 8 *Time history of the relative displacements of the structure*

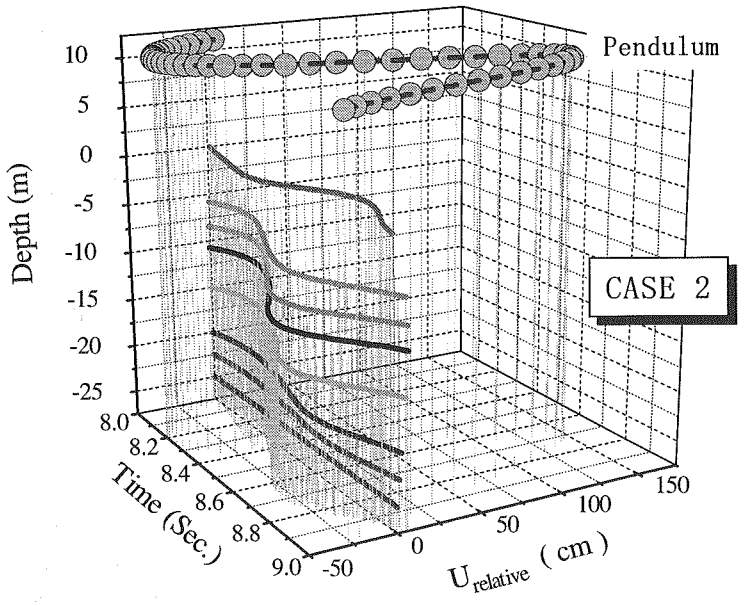

Fig. 9 *Time history of relative displacements with respect to the different elevations*

Fig. 8 shows the time histories of the relative displacement of the pendulum mass to the motion of the base layer beneath the embedment depth (-25m). It is clear from the figure that about 30% reduction of the peak values of displacement in case 1 is due to the decrease of the permeability of the surface soil fill. The effect of the permeability is much clearer at the level of the foundation top (0.0m). It is also noted in this figure that the time histories at different levels (the foundation top and the middle depth of embedment (-15m)) are out of phases each other. Fig. 9 shows the relative displacements of the structure with respect to the different elevations, it is found that the embedded body has the sharpest bent at the middle depth (-11m).

This numerical analysis clarifies a fact that it is quite possible that the response of a foundation embedded in completely saturated soil with high permeability is much smaller than the one with low permeability. Therefore, when a soil-structure interaction problem relates to a thick foundation with a large representative size embedded in water-saturated high-permeable soil deposit, the Poisson's ratio obtained by the in-situ PS logging should be modified in terms of the properties of the soil profiles.

CONCLUSIONS

Based on Biot's theory and the plane strain wave propagation model, a simple approach for analyzing the porous soil-structure interaction has been developed. In the present model, the porous soil medium surrounding the foundation of interest is sliced into a number of elements. Grasping the typical patterns of wave radiation through the sliced elements, the impedance functions for various vibration modes of the embedded disk are approximated by the syntheses of springs and dashpots. Since the springs and dashpots are independent of the excitement frequency, the present model is capable of analyzing the time-domain response of porous soil-structure systems. Assuming the case in which a coarse sandy surface soil layer overlies the subsurface material, the time-domain response of an inverted pendulum on an embedded upright Timoshenko beam is examined. Change in the permeability of the surface soil within a possible range yielded a noticeable difference in the response of the structure, because the solid-fluid interaction within the very surface layer has the greatest influence on the response of the structure.

REFERENCE

Nogami, T. and K.Konagai (1986). Time-domain axial response of dynamically loaded single piles, *J. eng. mech.* ASCE,**112**, 1241-1252.

Konagai, T. and T. Nogami (1987). Time-domain axial response of dynamically loaded pile groups, *J. eng. mech.* ASCE, **113**, 417-430.

Nogami, T. and K. Konagai (1988). Time-domain flexural response of dynamically loaded single piles, *J. eng. mech.* ASCE, **114**, 1512-1525.

Noorzad, A. and K. Konagai (1993). Comparison between resistances of porous and continuous model of saturated soil for plain strain case, *"SEISAN-KENKYU"*, I.I.S., University of Tokyo, **45**, 567-569.

Konagai,K. (1995). Simplified time-domain expression of soil response to transient loading, *Research report to Norwegian Institute of Technology, University of Trondheim,* Trondheim, Norway, 1-21.